V.M. Gun'ko

CONFINED SPACE EFFECTS ON VARIOUS LIQUIDS INTERACTING WITH FUMED NANOOXIDES AND POROUS SILICAS

Chuiko Institute of Surface Chemistry of National Academy of Sciences of Ukraine
17 General Naumov Str., Kyiv, 03164, Ukraine, E-mail: vlad_gunko@ukr.net

Interfacial phenomena at a surface of porous and highly disperse adsorbents in the systems containing strongly and weakly bound and unbound liquids depend strongly on the confined space effects. These effects as well as the temperature behavior of liquids located in pores or voids between nanoparticles depend on many factors. They are the pore size distributions, pore volume, specific surface area, surface chemistry of adsorbents, chemical structure and molecular sizes of adsorbates, accessibility of pores vs. probe molecule sizes, as well as textural instability of adsorbents. This instability can appear, e.g., as compaction of fumed oxides under action of liquid adsorbates, especially water, or due to mechanochemical activation. The aim of this study is to analyze features of the interfacial phenomena upon interactions of fumed oxides (silica, alumina, alumina/silica/titania) and porous silicas (silica gels and precipitated silica) with polar (water, dimethyl sulfoxide), weakly polar (chloroform), and nonpolar (n-decane, aromatic benzene and toluene) liquid adsorbates depending on the morphological and textural characteristics of the adsorbents, various adsorbate characteristics, and temperature. The observed effects as well as related phenomena are important because they can differently influence the efficiency of practical applications of adsorbents under various conditions (temperature, pressure, concentrations) depending on the characteristics of adsorbents and adsorbates (liquids, solvents and solutes).

Keywords: *fumed oxides, porous silicas, confined space effects, interfacial phenomena, bound liquids freezing/melting*

INTRODUCTION

Interfacial phenomena at a surface of solids with adsorbed gases/vapors, fluids, and liquids (including adsorption-desorption, dissolution, freezing, melting, boiling, evaporation, catalytic and other surface reactions, *etc*.) depend on features of confined space effects *vs*. pore sizes and temperature, surface and adsorbate structures, and a set of the textural characteristics of adsorbents [1–5]. These effects may be strongly different at the interfaces of highly disperse materials composed of nonporous nanoparticles (NPNP), *e.g*., fumed oxides, and material composed of porous micro/macroparticles (silica gels, mesoporous ordered silicas, zeolites, carbons, *etc*.) [6–28]. The interfacial phenomena are linked not only to technologically and industrially important properties and characteristics but also to biomedical ones, which differ for nano-, micro-, and macro-particles of such oxides as silica, alumina, and titania [1, 12–14, 29–32]. The interfacial phenomena depend strongly not only on the morphological, textural, and structural characteristics of sorbents

but also on the chemical composition, polarity, molecular weight, 1D, 2D, or 3D structures of adsorbates [27–39], as well as on various conditions: temperature, heating/cooling rate, pressure, interaction and equilibration time, pretreatment history, aging, *etc*. [1–3, 12, 27, 28, 33]. For example, the confined space effects result in the freezing/melting point depression ($\Delta T = T - T_{f(m)}$) for liquids located in pores. According to the Gibbs-Thomson relation [27, 40–45], the ΔT value depends on $T_{f(m)}$, the pore radius R (as $\sim 1/R$), bulk enthalpy of fusion (melting) ($1/\Delta H_{f(m)}$) of an adsorbate, density of a solid ($1/\rho$), energy of solid–liquid interactions (σ_{sl}), and some other parameters and characteristics. Only for a probe adsorbate without specific interactions with a solid surface and the same nature of adsorbents, *e.g*., silica gels, there is a simple correlation between the pore sizes and freezing (melting) point depression [27, 40–45]. As a whole, the pore shapes are non-ideal because they are characterized not only by different sizes, but also by various tortuosity and surface roughness [1–3, 20, 24, 27]. Therefore, real pores do not exactly correspond to any ideal

pore model such as cylindrical or slit-shaped one. For better description of the textural characteristics affecting the interfacial phenomena, several methods (adsorption-desorption, differential scanning calorimetry (DSC), small angle X-ray scattering (SAXS), cryoporometry, thermoporometry, relaxometry, microscopy, *etc*.) could be applied using different probes, *e.g*., polar and nonpolar, of larger and smaller molecular sizes, one- (*e.g*., Ar) or di-atomic (N_2), small (H_2O), plane (benzene), simple 3D (chloroform, alkanes, dimethyl sulfoxide (DMSO)), *etc*. In this study, nitrogen adsorption, transmission electron microscopy (TEM) and DSC (with various probes: polar water and DMSO, weakly polar chloroform, and nonpolar benzene, toluene, and *n*-decane) methods are applied to fumed oxides (silica, alumina, ternary alumina/silica/titania) and porous silicas (silica gels and precipitated silica) for comparative analysis of various factors affecting the interfacial behavior of polar, weakly polar and nonpolar adsorbates.

MATERIALS AND METHODS

Various silicas: fumed silicas A-500 and A−300 (Pilot plant of Chuiko Institute of Surface Chemistry (PPCISC), Kalush, Ukraine), precipitated silica Syloid® 244 (Grace Davidson), silica gels Si-40, Si-60, and Si-100 (Merck) with various specific surface area (Table 1, S_{BET}) were used as the initial materials. Additionally, fumed alumina and ternary alumina/silica/titania AST1

with 10, 89, and 1 wt. % of silica, alumina, and titania, respectively (Table 1) were used as the initial powders (PPCISC). Mechanochemical activation (MCA) of fumed silica A−300 was performed in a ceramic ball-mill (volume 1 dm³ 2/3 filled by balls of 2–3 cm in diameter, 60 rpm) using for 6 h. AST1 alone and a blend with A−300 and AST1 (1:1) were treated in a stainless-steel grinder (30 W, 50 Hz, volume 10 cm³ with a stainless-steel ball of 0.8 cm in diameter) for 30 min. Various characteristics of fumed oxides, silica gels and precipitated silica were described in detail elsewhere [27, 28, 33–39]. The X-ray diffraction data for fumed oxides used here were described in detail elsewhere [27, 28, 33, 46].

TEXTURAL CHARACTERISTICS

The textural characteristics of adsorbents (degassed at 473 K for 2 h) were determined using low-temperature (77.4 K) nitrogen adsorption–desorption isotherms recorded using Micromeritics ASAP 2405N or ASAP 2420 (V2.09 J) or Quantachrome Autosorb adsorption analyzers. The specific surface area (Table 1, S_{BET}) was calculated according to the standard BET method [3] using the pressure range $p/p_0 = 0.05$–0.3 (where p and p_0 denote the equilibrium and saturation pressure of nitrogen at 77.4 K, respectively) and 0.162 nm² as an area occupied by a nitrogen molecule. The total pore volume (V_p) was evaluated from the nitrogen adsorption at $p/p_0 = 0.98$–0.99 [24].

Table 1. Textural characteristics of adsorbents

Sample	S_{BET}, m²/g	S_{nano}, m²/g	S_{meso}, m²/g	S_{macro}, m²/g	V_p, cm³/g	V_{nano}, cm³/g	V_{meso}, cm³/g	V_{macro}, cm³/g
A-500 initial	492	260	216	16	0.874	0.067	0.588	0.219
A-500 aged	331	24	254	54	1.207	0.005	0.372	0.830
A−300 initial	330	47	259	24	0.917	0.018	0.418	0.481
A−300, MCA 6 h	300	162	136	2	0.773	0.121	0.597	0.055
Al_2O_3	70	21	41	8	0.181	0.003	0.071	0.107
AST1 initial	100	34	57	9	0.254	0.006	0.115	0.133
AST1 aged	78	25	44	9	0.234	0.005	0.097	0.132
AST1 aged, MCA	60	12	39	8	0.308	0.003	0.142	0.163
A-300/AST1 (1:1)	184	93	74	17	0.481	0.018	0.251	0.213
Syloid 244	336	39	291	6	1.591	0.022	1.457	0.112
Si-40	732	188	433	1.4	0.636	0.077	0.493	0.066
Si-60	456	0	456	0.2	0.822	0	0.818	0.004
Si-100	349	65	284	0.2	1.224	0.020	1.198	0.006

Note. The V_{nano} and S_{nano} values were calculated by integration of the $f_V(R)$ and $f_S(R)$ function, respectively, at pore radius of 0.35 nm < R < 1 nm, V_{meso} and S_{meso} at 1 nm < R < 25 nm, and V_{macro} and S_{macro} at 25 nm < R < 100 nm

The nitrogen adsorption-desorption isotherms were used to compute the pore size distributions (PSD, differential $f_V(R)$ ~ dV_p/dR and $f_S(R)$ ~ dS/dR) using a complex approach with a model of slit-shaped and cylindrical pores and voids between NPNP (SCV or CV) and density functional theory (DFT) method with a self-consistent regularization (SCR) procedure described in detail elsewhere [47]. Additionally, nonlocal DFT (NLDFT) method with cylindrical pores in silica (equilibrium model, Quantachrome software) was applied to porous silicas to compute the differential PSD. The $f_{V,S}(R)$ functions were used to compute contributions of nanopores (V_{nano} and S_{nano}, Table 1) at pore radius of 0.35 nm < R < 1 nm, mesopores (V_{meso} and S_{meso}) at 1 nm < R < 25 nm, and macropores (V_{macro} and S_{macro}) at 25 nm < R < 100 nm. Some additional information on the textural and other characteristics of fumed oxides and other adsorbents could be found elsewhere [27, 28, 33–39, 47–51].

TRANSMISSION ELECTRON MICROSCOPY

Transmission electron microscopy (TEM) images of oxide adsorbents have been recorded with a BS 540 (Tesla) apparatus (accelerating voltage 80 kV, resolution 0.8 nm) and JEM–2100F apparatus (Japan, 200 kV). Powders sample were added to acetone (for chromatography) and sonicated. Then a drop of the suspension was deposited onto a copper grid with a thin carbon film. After acetone evaporation, sample particles remained on the film were studied with TEM. TEM images were analyzed to compute the particle size distributions (PaSD) using such software as ImageJ (granulometry plugin) [52] and Fiji (local thickness plugin) [53].

DIFFERENTIAL SCANNING CALORIMETRY

Differential scanning calorimetry (DSC) investigations of interactions of fumed oxides, silica gels and precipitated silica with such nonpolar liquids as *n*-decane (melting point T_m = 242.7–244.0 K), aromatic benzene (T_m = 278.7 K) and toluene (T_m = 178.2 K), weakly polar chloroform (T_m = 209.7 K), and polar water (T_m = 273.15 K) and dimethyl sulfoxide (DMSO, T_m = 291.7 K) were carried out using a PYRIS Diamond (Perkin Elmer Instruments, USA) differential scanning

calorimeter. It was calibrated at different heating rates using standard samples such as ultrapure water (melting temperature T_m = 273.15 K) and indium (T_m = 429.75 K) supplied by the producer and using the recommended standard calibration procedure. Water was purified on a Milli-Q system from Millipore (Millipore, Bedford, MA, USA). The samples were closed in the aluminum cells. The weight of liquid adsorbates was 2–4 times greater than the weight of solid samples. As a control, an empty aluminum crucible was used. Measurements were carried out in an atmosphere of inert gas (helium). In order to prevent the system defrosting, nitrogen was used as a curtain gas. Experiments were performed at a rate of temperature change of 10 K min^{-1}. Heating thermograms were registered in the 193–293 K range. Here only shifted DSC curves for heating run (after cooling run) are shown to simplify the analysis of the confined space effects. Some additional results for similar systems could be found elsewhere [27, 28, 33–39].

RESULTS AND DISCUSSION

Fumed oxides representing very loose powders (Fig. 1) at the bulk density ρ_b = 0.04–0.14 g/cm^3 (dependent on the PaSD and true density of nanoparticles) composed of NPNP forming aggregates and agglomerates of aggregates possess the textural porosity with voids between nanoparticles in secondary and ternary structures [27, 28, 33].

Contacts between adjacent NPNP are not very strong and can be changed by any external action such as mechanochemical activation (MCA) with pressing, ball-milling, hydro-compaction, *etc*. [27, 28, 33] (Figs. 1 *c* – 3, Table 1). For example, if the amounts of water *h* > 1.5 g per gram of A−300 that hydro-compaction leads to significant changes in the textural characteristics [48]. If a liquid is hydrophobic (benzene, toluene, alkanes) that a similar effect is weak [27, 28]. The effects of alcohols are weaker than that of water alone or water/alcohol mixtures [27].

Fumed alumina (Fig. 1 *e*) and AST1 (Fig. 1 *f*) are composed of NPNP with a broader distribution of sizes than that of A−300 (Fig. 2). Typically, the lower the specific surface area (larger average NPNP sizes), the broader the particle size distribution [27, 54]. Fumed silica nanoparticles (5–15 nm in size for A−300) are amorphous and composed with smaller nuclei

(Figs. 2 *a* (curve 3) and 2 *c*) formed during flame synthesis. Large nanoparticles of fumed alumina and AST1 (mainly (89 wt. %) with alumina) are polycrystalline because maximal sized of crystallites (crystallite size distributions, CSD) computed using X-ray diffraction (XRD) patterns (as described previously [46]) are much smaller (Fig. 2 *c*) than maximal sizes of nanoparticles (Fig. 2 *b*, *d*).
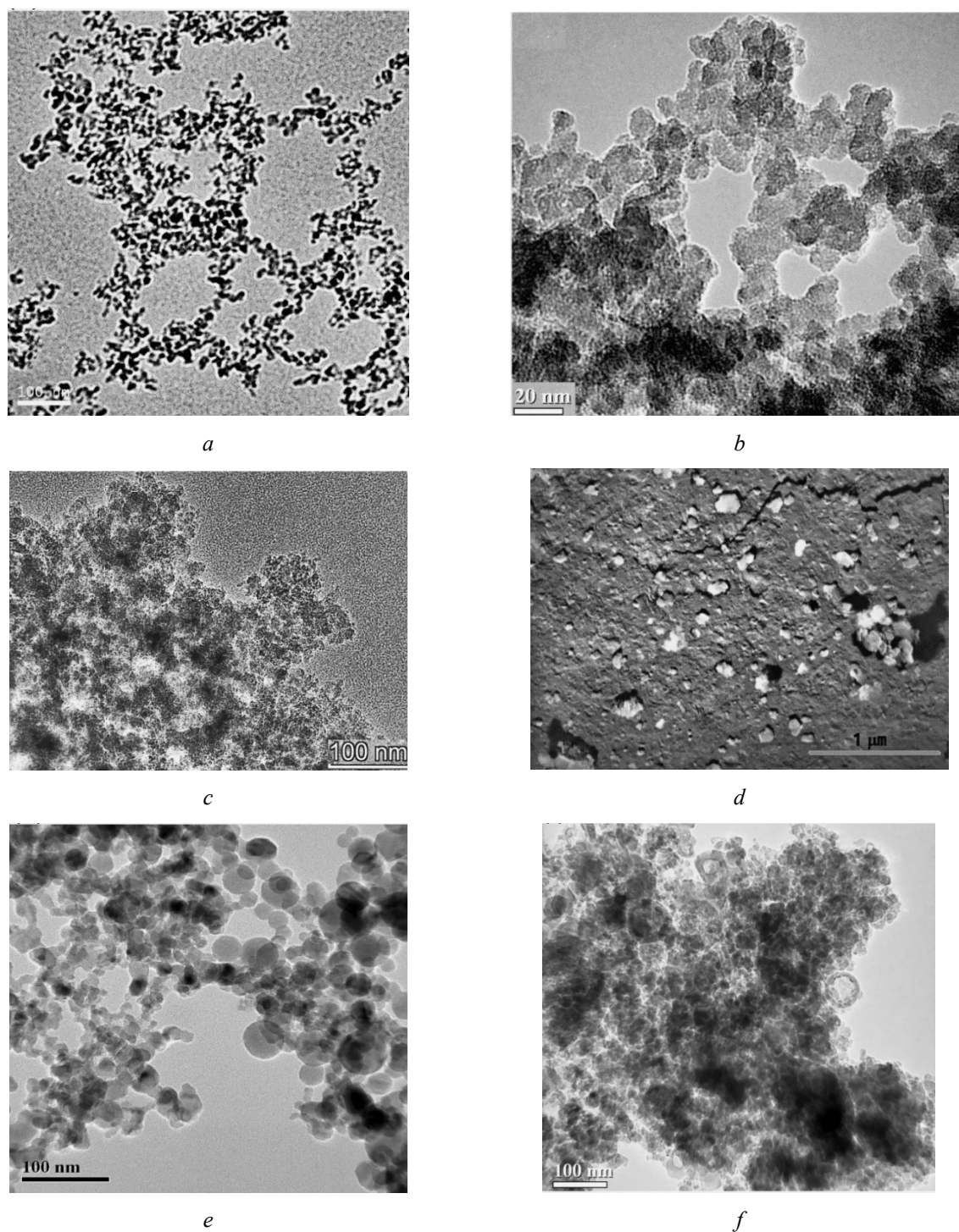

Fig. 1. TEM images of A−300 (*a*, *b*) initial and (*c*) compacted, (*d*) Si−40, (*e*) fumed alumina, and (*f*) AST1 (scale bar (*a*, *c*, *e*, *f*) 100 nm, (*b*) 20 nm, and (*d*) 1 µm)
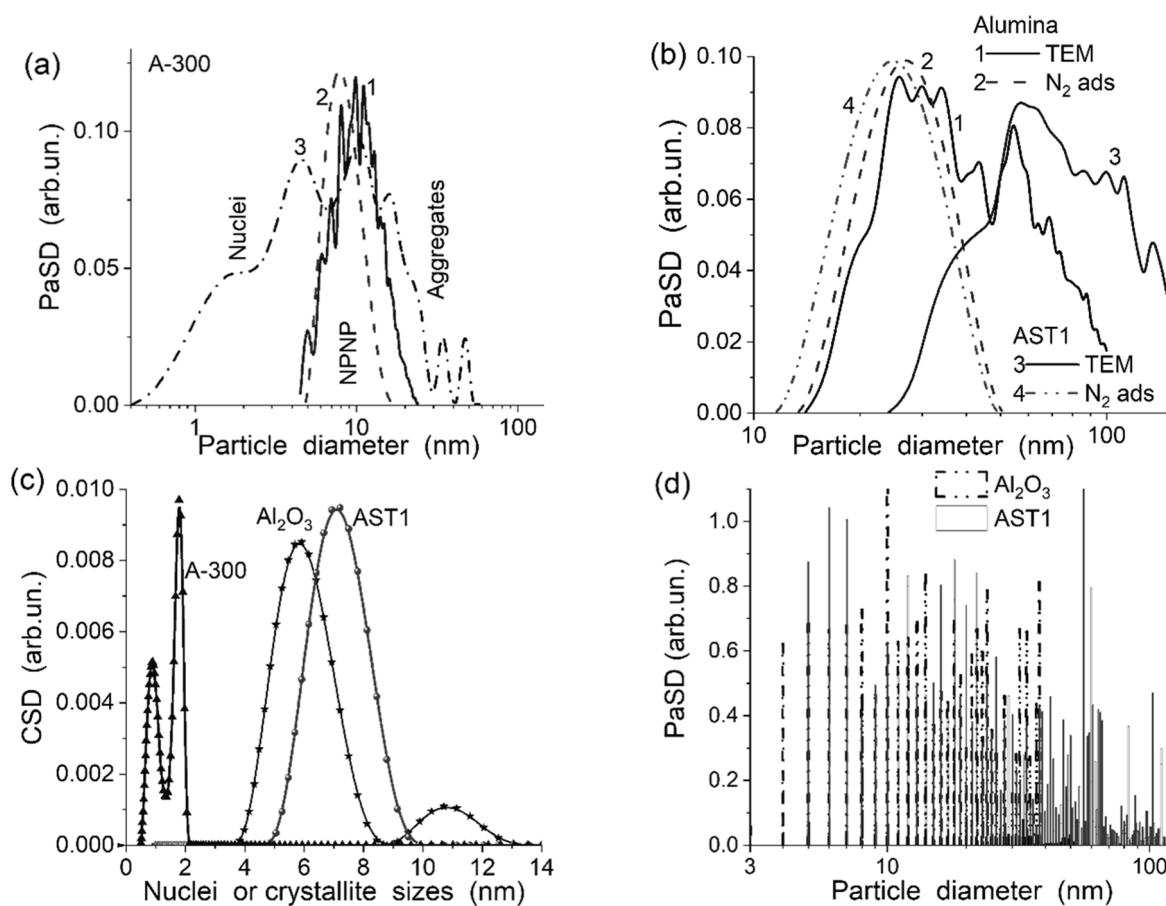
Fig. 2. Particles, nuclei, and crystallite size distributions (PaSD, CSD) for fumed (*a*) A−300 (curves 1-3), (*b*) Al_2O_3 (1, 2) and AST1 (3, 4) computed using nitrogen adsorption isotherms (*a* 2, *b* 2 and 4), TEM images (granulometry plugin [52]) (*a* 1, *b* 1 and 3), SAXS (*a* 3); (*c*) XRD patterns with full profile analysis of the main lines for A−300, alumina, and AST1; and (*d*) TEM images (local thickness plugin [53]) for alumina and AST1

This particulate morphology of fumed oxides can play a certain role upon their textural changes in the powders under external actions (mechanical, adsorption, hydro-compaction, *etc.*). It should be noted that simple aging of the fumed oxide powders can lead certain textural changes (Fig. 3 *b*). These changes are greater for fumed silica (*e.g.*, Fig. 3 *b*, A−500, S_{BET} decreases for 33 %, but V_p increases for 38 %) than for fumed oxides with crystalline phases (*e.g.*, AST1, S_{BET} decreases for 22 %, V_p decreases for 8 %) [27, 54]. In contrast to fumed oxides, particles of silica gels and precipitated silica are relatively (texturally) stable in comparison to aggregates and agglomerates of fumed oxides [1, 12–14]. The PSD of porous silicas are broader (Fig. 3 *d*) with increasing pore sizes and decreasing the specific surface area (Table 1); however, it is narrower than the PSD of fumed oxides (Fig. 3 *a–c*). Thus, in this study, some materials are texturally 'soft'

(fumed oxides) but others (porous silicas) are relatively rigid and texturally stable under external actions. This aspect can appear upon interactions with various liquid adsorbates, especially if their amounts are greater than pore volume (porous adsorbent) and adsorbent weight (fumed oxides).

To fill pores (porous silicas) completely or to provide the compaction effects for 'soft' powders (fumed oxides), the amounts of liquids used during the DSC measurements were two-four times greater than the mass of solid adsorbents. Besides the textural effects (with respect to PSD, porosity, V_p and S_{BET} values affected by MCA, compaction, *etc.*), it is possible several other effects caused by the different surface structures of silicas, alumina, and AST1. Various surface sites (*e.g.*, terminal and bridging hydroxyls, incomplete O-coordinated Al and Ti atoms) can differently interact with polar and nonpolar

adsorbates affected by confined space in voids between NPNP or in pores of silica gels. Liquid adsorbates can be in several states such as strongly and weakly bound and unbound ones [27]. The first one corresponds to liquids located in narrow pores (nanopores and narrow

mesopores) or at the first surface layer. Weakly bound liquids are located in broad mesopores and macropores. Unbound liquids (having the characteristics similar to bulk liquids) are located in macropores or out of pores.
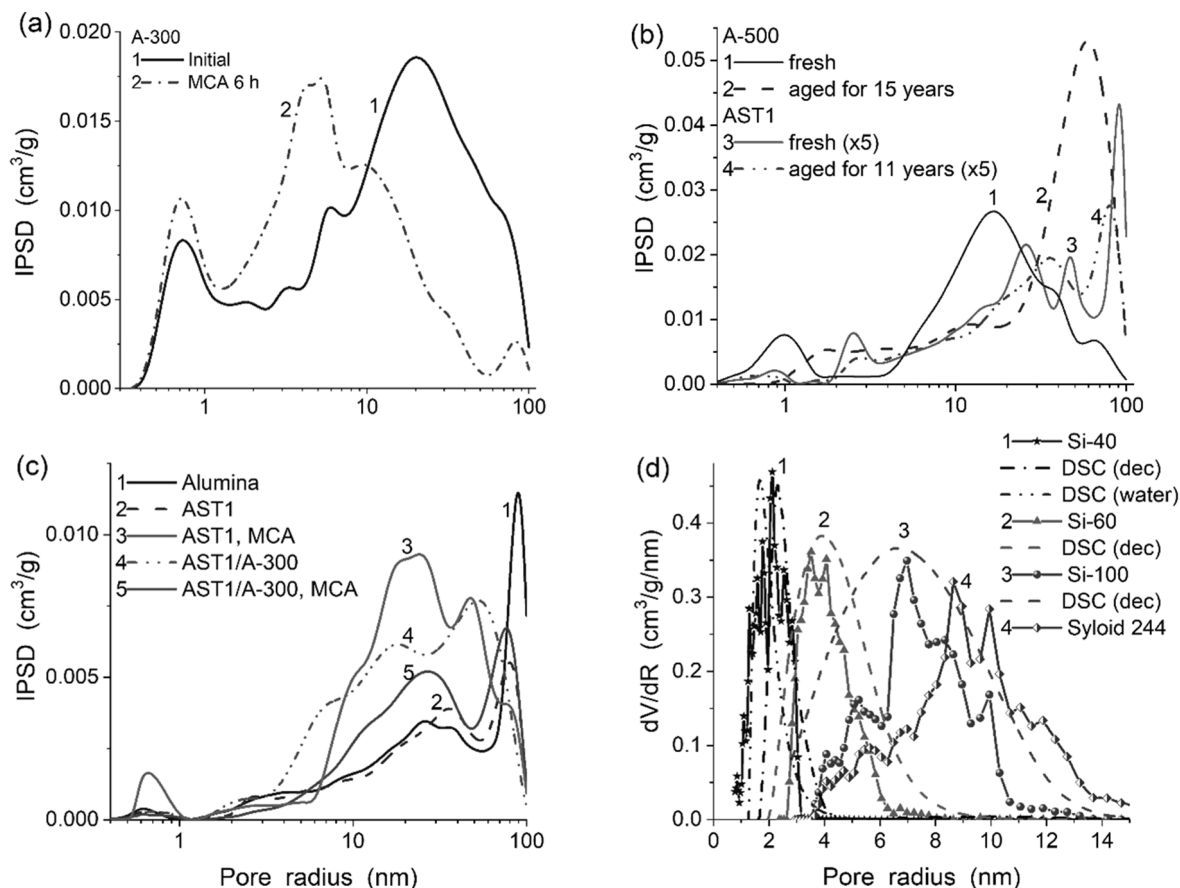

Fig. 3. Incremental (*a–c*) and (*c*) differential DFT PSD, (*a–c*) SCV/SCR DFT of initial and pretreated (MCA or aged) oxides and (*d*) NLDFT of non-pretreated porous silicas (solid lines, textural characteristics are in Table 1); DSC PSD (dashed lines) calculated using the Gibbs-Thomson relation for the melting point depression with *n*-decane (dec) and water as probes

For A−300 initial (Fig. 4 *a*) and after MCA (Fig. 4 *b*), a minimal value of the melting point depression (MPD) is observed for water. This can be explained by several effects. First, interactions of water – water and water – surface hydroxyls are characterized by similar energies. Second, water tends to be adsorbed as clusters. Third, water can strongly change the organization of secondary and ternary structures with NPNP of fumed oxides. As a whole, a MPD sequence for A−300 is water < toluene < *n*-decane < benzene < chloroform < DMSO, and a similar one is for A−300 MCA.

There are several factors resulting in changes in the MPD effects for various liquids: (i) difference in the interactions (Gibbs free energy, ΔG) of molecule-molecule and molecule-solid surface; (ii) various size-dependent accessibility of pores and voids for molecules of different adsorbates; (iii) adsorbate/adsorbent weight ratio affecting pore/void filling and amounts of strongly and weakly bound and unbound liquids; (iv) textural changes of adsorbents (with bound adsorbates) during cooling/heating; (v) differences in the effects of the same cooling/heating rate for different adsorbates with

different ΔG values of melting. Therefore, the MPD sequence for A−300 does not correspond to a sequence with the condensation heat (which characterizes the molecule-molecule interactions in liquids) $\Delta H_{con} = -31.3, -33.8, -37.0, -45.0, -51.3,$ and -52.9 kJ/mol for chloroform, benzene, toluene, water, n-decane, and DMSO, respectively. Melting peaks located at $T > T_m$ (Figs. 4 and 5, $T - T_m > 0$) are due to melting delay for frozen liquids located out of pores (voids) or located in macropores (macrovoids). This melting delay effect is caused by a relatively high heating rate (10 K/min) and relatively great amounts of liquids that are several times larger than the pore volume. Re-calculation (to approach to their behavior in pores/voids) of the ΔH_{con} values per cm^3 (as $\Delta H_{con}/MW/\rho$) gives $-0.49, -0.46, -0.49,$ $-0.18, -0.62,$ and -2.50 kJ/cm^3, respectively, that does not correspond to the MPD sequence too.

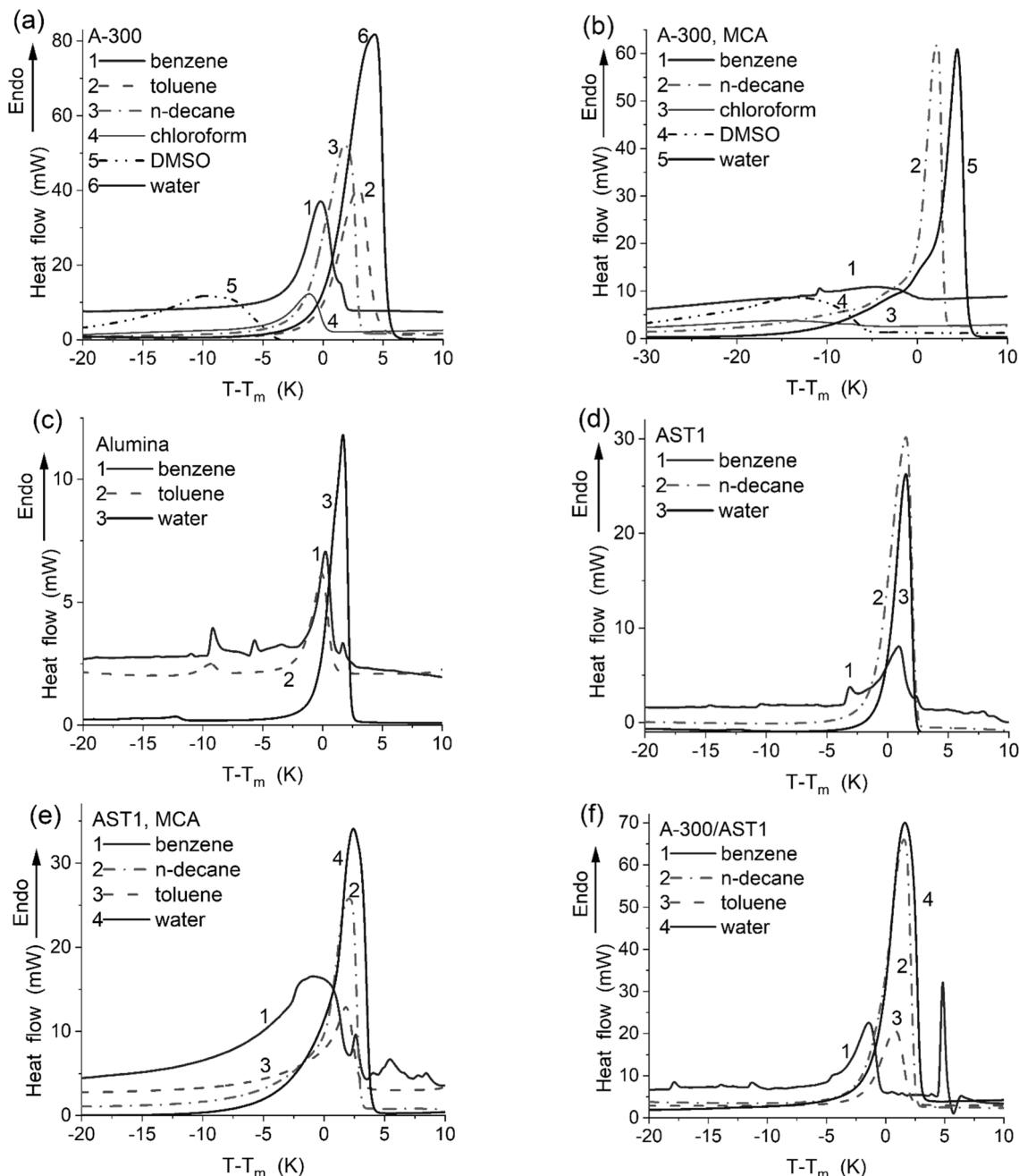**Fig. 4.** Shifted (T-T_m) DSC curves for various liquids bound to nanooxides: (*a*) A−300, (*b*) A−300 after MCA for 6 h, (*c*) alumina; (*d*) alumina/silica/titania AST1, (*e*) AST1 after MCA, and (*f*) blend with A−300 and AST1
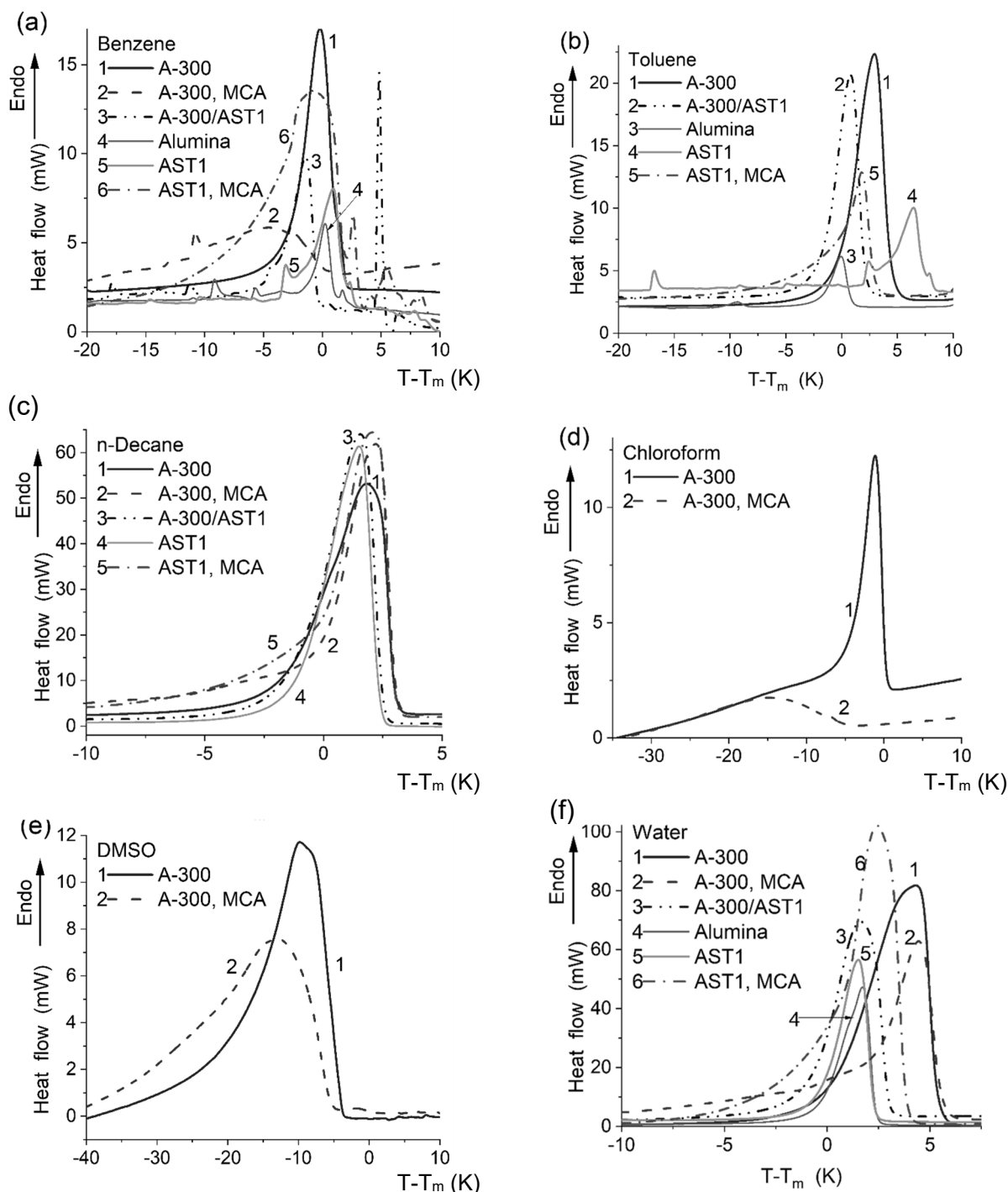
Fig. 5. Shifted (T–T_m) DSC curves for various liquids: (*a*) benzene, (*b*) toluene, (*c*) *n*-decane, (*d*) chloroform, (*e*) DMSO, and (*f*) water bound to nanooxides

Thus, the condensation heat of liquids is not a single characteristic of adsorbates mainly affecting the difference in their melting (freezing) point depression in pores of the same adsorbents. Minimal ΔT values are also observed for water upon interaction with other fumed oxides (Fig. 4 *d–f*). However, the effects increase after MCA treatments of fumed oxides (Fig. 5). Additionally, it is greater for more polar oxides (AST1, alumina, especially for AST1 after MCA) than that for fumed silica. The MPD effects are minimal for the most nonpolar *n*-decane (Fig. 5 *c*) in comparison to other organic adsorbates (Fig. 5). The MPD effects are greater for aromatic

benzene (Fig. 5 *a*) with plane (2D) molecules than that for toluene (molecules with a small 3D tail, CH$_3$) (Fig. 5 *b*). The behavior of chloroform and DMSO bound to A−300 MCA differs from that for initial A−300 (Fig. 5 *d, e*) due to increased

confined space effects in narrower mesopores (Fig. 3 *a*) and other changes in the textural characteristics (Table 1). The effects for water are stronger for AST1 MCA than for A−300 MCA in comparison to the initial fumed oxides (Fig. 5 *f*).
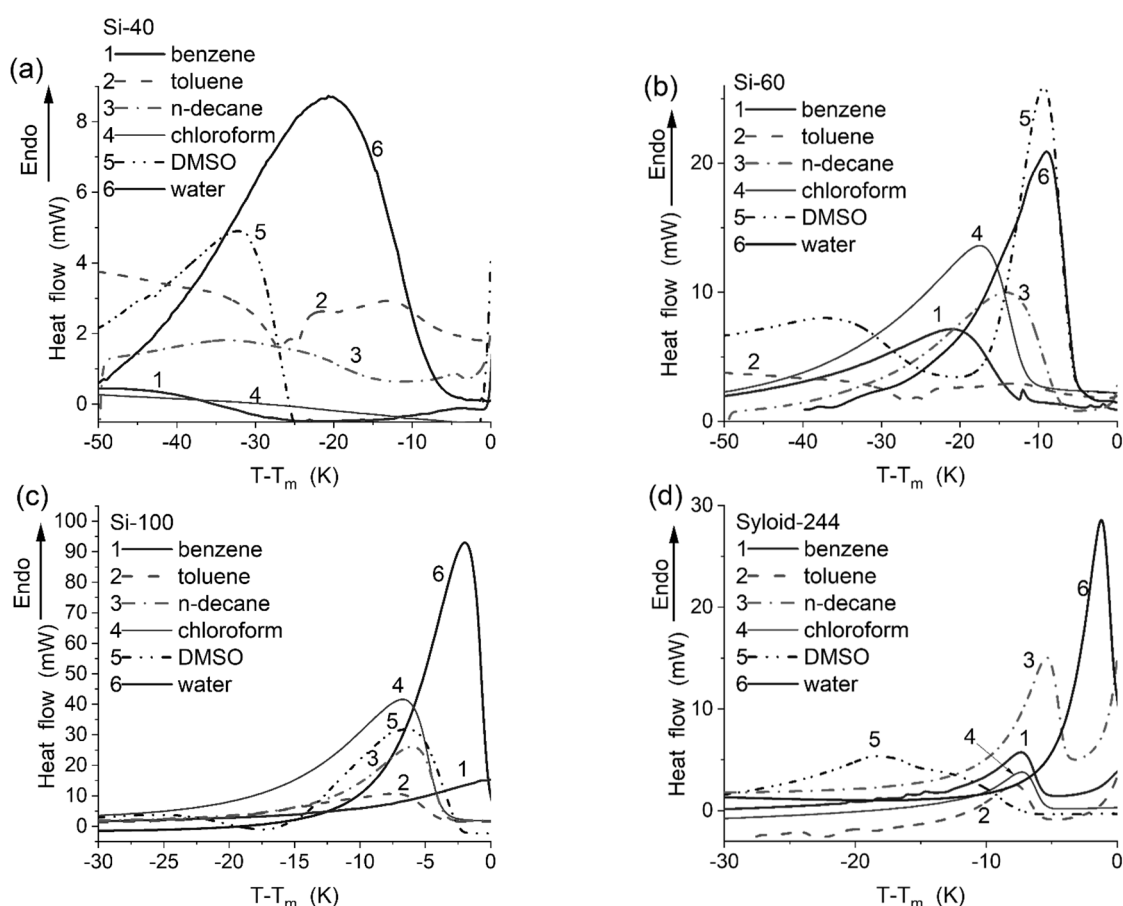

Fig. 6. Shifted (T–T_m) DSC curves for various liquids bound to such porous silicas as silica gels: (*a*) Si−40, (*b*) Si−60, (*c*) Si−100, and (*d*) precipitated silica Syloid 244

For porous adsorbents, the MPD effects depend strongly on the pore sizes and volume (Figs. 3, 6, and 7, Table 1). It could be expected that the MPD effect should be maximal for Si−40 (Fig. 6 *a*) with minimal pore sizes. However, the minimal pore volume for Si−40 (Table 1, V_p) results in minimal energetic effects since the heat flow increases with increasing V_p value (Fig. 6) and a ratio between the adsorbate amount and pore volume decreases with increasing V_p value for Si−60, Si−100, and Syloid 244. Additionally, Si−40 pore filling by nonpolar or weakly polar adsorbates (Fig. 7 *a–d*) can be incomplete (*e.g.*, due to air bubbles remaining in narrow pores).

Polar adsorbates (DMSO and water) can better fill pores of hydrophilic Si−40 (Fig. 7 *e, f*)

than weakly polar or nonpolar organic liquids (Fig. 7 *a–d*). The MPD effect for water more strongly decreases with increasing pore sizes and pore volume of silicas (Figs. 6 and 7 *f*). A similar effect is for other adsorbates, but it is less strong (Fig. 7 *a–e*). As a whole, for Si−60 and Syloid 244, the MPD sequence is water < *n*-decane < chloroform < benzene < toluene < DMSO, but it differs for Si−40 and Si−100 possessing narrower and broader mesopores (Figs. 6 and 7) or for fumed oxides (Figs. 4 and 5). For fumed oxides, the MPD effect is much weaker than that for silica gels, especially Si-40 with narrow pores (Fig. 3). This is explained by a small contribution of nanopores and narrow mesopores (voids) into the PSD of fumed oxides

in contrast to Si-40 or Si-60 (Fig. 3). For water, a correlation of pore sizes of silica gels (Fig. 3 *d*) and the MPD effect (Fig. 7 *f*) is well visible. For other adsorbates, there is a similar tendency (Fig. 7 *a–e*) but less clear due to overlapping several effects above mentioned. Therefore, for porous silicas, NMR cryoporometry and DSC thermoporometry with water as a probe give the PSD being in a better agreement with the textural characteristics calculated using nitrogen adsorption data than that for fumed oxides

[27, 34, 39, 49, 50]. This difference can be additionally affected by the textural instability of fumed oxides that more strongly appears upon interactions with water than with nitrogen or organic liquids [27]. However, the DSC or NMR probes without specific interactions with adsorbents are more appropriate for the textural characterization of porous (Fig. 3 *d*) or disperse adsorbents with the thermoporometry or cryoporometry than water as a probe [27, 28, 33, 55].
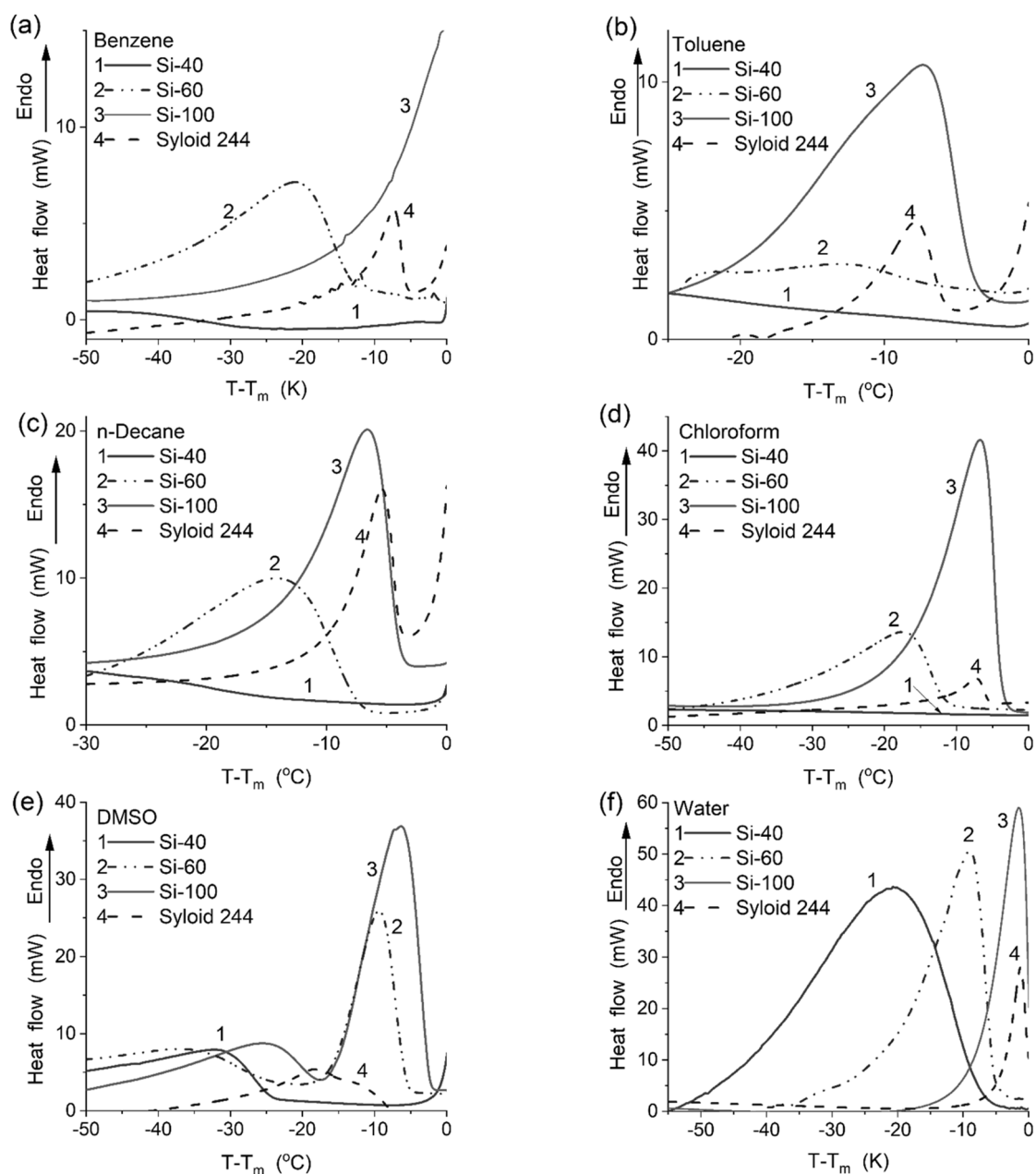

Fig. 7. Shifted ($T–T_m$) DSC curves for (*a*) benzene, (*b*) toluene, (*c*) *n*-decane, (*d*) chloroform, (*e*) DMSO, and (*f*) water bound to porous silicas

CONCLUSION

The confined space effects for liquids located in pores (or voids between NPNP) depend on many factors such as the pore size distribution and pore volume, surface chemistry of adsorbents and chemical structure of adsorbates, molecular sizes of adsorbates and accessibility of pores, the degree of narrow pore filling by adsorbates, textural instability of adsorbents, *e.g.*, compaction of fumed oxides under action of liquid adsorbates, especially water, or due to mechanochemical activation. Some features of these phenomena have been elucidated under the analysis of the interactions of fumed oxides (silica, alumina, alumina/silica/titania) and porous silicas (silica gels and precipitated silica) with polar (water, DMSO), weakly polar (chloroform), and nonpolar (*n*-decane, aromatic benzene and toluene) liquid adsorbates. The MPD sequence for A−300 is water < toluene < *n*-decane < benzene < chloroform < DMSO, and a similar one is for A−300 after MCA. For porous Si−60 and Syloid 244, the MPD sequence is different water < *n*-decane < chloroform < benzene < toluene < DMSO. It also differs for Si−40 and Si−100 possessing narrower and broader mesopores, as well as for fumed oxides. The observed MPD sequences do not correspond to a single characteristic such as polarity, molecular weights, condensation heat and other individual characteristics of adsorbates. It can be also dependent on the textural changes of fumed oxides upon interactions with liquids, especially polar such as water. In other words, the observed phenomena related to the MPD are affected by many factors and cannot be described on the basis of any single characteristic of an adsorbate or an adsorbent. Thus, changes in the confined space effects result in different and complex influences onto various liquids located in different pores or voids between NPNP. However, a simple correlation could be observed for water (or some other adsorbates) interacting with very similar adsorbents (*e.g.*, silica gels) different only in the pore size distributions, S_{BET} and V_p values. The observed effects as well as related phenomena are important because they can differently influence the efficiency of practical applications of adsorbents under various conditions (temperature, pressure, concentrations) depending on a set of the characteristics of adsorbents and adsorbates (liquids/solvents and solutes).

Ефекти обмеженого простору для різних рідин, що взаємодіють з пірогенними нанооксидами та пористими кремнеземами

В.М. Гунько

Інститут хімії поверхні ім. О.О. Чуйка Національної академії наук України
вул. Генерала Наумова, 17, Київ, 03164, Україна, vlad_gunko@ukr.net

Міжфазні явища для сильно та слабко зв'язаних рідких адсорбатів, локалізованих в порах пористих або високодисперсних адсорбентів, сильно залежать від ефектів обмеженого простору. Ці ефекти, а також температурна поведінка рідких адсорбатів, розташованих в порах, залежать від багатьох чинників, як розміри пор та адсорбованих молекул, текстурна нестабільність адсорбентів (наприклад, ущільнення пірогенних оксидів під дією рідких адсорбатів, особливо води, або через механохімічну активацію) тощо. Метою даного дослідження є аналіз особливостей взаємодії пірогенних оксидів (діоксид кремнію, оксид алюмінію, оксид алюмінію/кремнезем/діоксид титану) з полярним (вода, диметилсульфоксид), слабкополярними (хлороформ, ароматичні бензол та толуол) і неполярними (н-декан) рідкими адсорбатами в

залежності від морфологічних і текстурних характеристик адсорбентів та температури. Ці ефекти, а також пов'язані явища, є важливими, оскільки вони можуть по-різному впливати на ефективність практичних застосувань адсорбентів при різних умовах (температура, тиск, концентрація) залежно від характеристик адсорбентів та адсорбатів (рідин/розчинників та розчинених сполук).

Ключові слова: пірогенні оксиди, пористі кремнеземи, ефекти обмеженого простору, явища на межах поділу, заморожування/розморожування зв'язаних рідин

REFERENCES

1. Somasundaran P. *Encyclopedia of Surface and Colloid Science*. Third Edition. (Boca Raton: CRC Press, 2015).
2. Yang R.T. Adsorbents: Fundamentals and Applications. (New York: Wiley, 2003).
3. Adamson A.W., Gast A.P. *Physical Chemistry of Surface*. 6th edition. (New York: Wiley, 1997).
4. Slejko F.L. Adsorption Technology: A Step-by-Step Approach to Process Evaluation and Application. (New York: Marcel Dekker Inc., 1985).
5. Birdi K.S. *Handbook of Surface and Colloid Chemistry*. Third edition. (Boca Raton: CRC Press, 2009).
6. *Ullmann's Encyclopedia of Industrial Chemistry*. (Weinheim: Wiley-VCH, 2008).
7. *Basic Characteristics of AEROSIL® Fumed Silica.* Technical Bulletin Fine Particles. N 11. (Hanau: Evonik Industries AG, 2006).
8. Lu K. Nanoparticulate Materials. Synthesis, Characterization, and Processing. (Hoboken, New Jersey: John Wiley & Sons, Inc., 2013).
9. Moreno-Piraján J.C., Giraldo-Gutierrez L., Gómez-Granados F. *Porous Materials Theory and Its Application for Environmental Remediation*. (Cham: Springer Nature, 2021).
10. Rousseau R.W. *Handbook of Separation Process Technology*. (New York: John Wiley & Sons, 1987).
11. Schweitzer P.A. *Handbook of Separation Techniques for Chemical Engineers*. 2nd ed. (New York: McGraw-Hill Inc., 1988).
12. Iler R.K. *The Chemistry of Silica*. (Chichester: Wiley, 1979).
13. Legrand A.P. *The Surface Properties of Silicas*. (New York: Wiley, 1998).
14. Bergna H.E., Roberts W.O. *Colloidal Silica: Fundamentals and Applications*. (Boca Raton: CRC Press, 2006).
15. Tapia O., Bertrán J. *Solvent Effects and Chemical Reactivity*. (New York: Kluwer Academic Publishers, 2000).
16. Henderson M.A. The interaction of water with solid surfaces: fundamental aspects revisited. *Surf. Sci. Rep.* 2002. **46**(1): 1.
17. Al-Abadleh H.A., Grassian V.H. Oxide surfaces as environmental interfaces. *Surf. Sci. Rep.* 2003. **52**(3–4): 63.
18. Auroux A. Microcalorimetry methods to study the acidity and reactivity of zeolites, pillared clays and mesoporous materials. *Top. Catal.* 2002. **19**(3): 205.
19. Campbell C.T., Sellers J.R.V. Enthalpies and entropies of adsorption on well-defined oxide surfaces: Experimental measurements. *Chem. Rev.* 2013. **113**(6): 4106.
20. Eder F., Lercher J.A. On the role of the pore size and tortuosity for sorption of alkanes in molecular sieves. *J. Phys. Chem. B*. 1997. **101**(8): 1273.
21. Gounder R., Iglesia E. The catalytic diversity of zeolites: Confinement and solvation effects within voids of molecular dimensions. *Chem. Commun*. 2013. **49**(34): 3491.
22. Chorkendorff I., Niemantsverdriet J.W. *Concepts of Modern Catalysis and Kinetics*. (Weinheim: John Wiley & Sons, 2006).
23. Dauenhauer P.J., Abdelrahman O.A. A universal descriptor for the entropy of adsorbed molecules in confined spaces. *ACS Cent. Sci*. 2018. **4**(9): 1235.
24. Gregg S.J., Sing K.S.W. *Adsorption, Surface Area and Porosity*. 2nd ed. (London: Academic Press, 1982).
25. Wypych G. *Handbook of Solvents*. (Toronto: ChemTec Publishing, 2001).
26. Kammerhofer J. *Capillary Wetting of Heterogeneous Powders*. 1st edn. (Göttingen: Cuvillier Verlag, 2019).
27. Gun'ko V.M., Turov V.V. Nuclear Magnetic Resonance Studies of Interfacial Phenomena. (Boca Raton: CRC Press, 2013).
28. Gun'ko V.M., Turov V.V., Zarko V.I., Goncharuk O.V., Pahklov E.M., Skubiszewska-Zięba J., Blitz J.P. Interfacial phenomena at a surface of individual and complex fumed nanooxides. *Adv. Colloid Interface Sci.* 2016. **235**: 108.
29. Brunelli A., Pojana G., Callegaro S., Marcomini A. Agglomeration and sedimentation of titanium dioxide nanoparticles (n-TiO_2) in synthetic and real waters. *J. Nanopart. Res*. 2013. **15**(6): 1684.

30. Canesi L., Ciacci C., Vallotto D., Gallo G., Marcomini A., Pojana G. In vitro effects of suspensions of selected nanoparticles (C_{60} fullerene, TiO_2, SiO_2) on Mytilus hemocytes. *Aquat. Toxicol.* 2010. **96**(2): 151.

31. D'Agata A., Salvatore F., Dallas L.J., Fisher A.S., Maisano M., Readman J.W., Jha A.N. Enhanced toxicity of 'bulk' titanium dioxide compared to 'fresh' and 'aged' nano-TiO_2 in marine mussels (Mytilus galloprovincialis). *Nanotoxicology.* 2014. **8**(5): 549.

32. Srikanth K., Mahajan A., Pereira E., Duarte A.C., Rao J.V. Aluminium oxide nanoparticles induced morphological changes, cytotoxicity and oxidative stress in Chinook salmon (CHSE-214) cells. *J. Appl. Toxicol.* 2015. **35**(10): 1133.

33. Gun'ko V.M., Turov V.V., Zarko V.I., Goncharuk O.V., Pakhlov E.M., Matkovsky O.K. Interfacial phenomena at a surface of individual and complex fumed nanooxides. *Surface.* 2019. **11(26)**: 3.

34. Gun'ko V.M. Interfacial phenomena: effects of confined space and structure of adsorbents on the behavior of polar and nonpolar adsorbates at low temperatures. *Current Physical Chemistry.* 2015. **5**(2): 137.

35. Turov V.V., Gun'ko V.M., Pakhlov E.M., Krupska T.V., Tsapko M.D., Charmas B., Kartel M.T. Influence of hydrophobic nanosilica and hydrophobic medium on water bound in hydrophilic components of complex systems. *Colloids Surf., A.* 2018. **552**: 39.

36. Gun'ko V.M., Pakhlov E.M., Goncharuk O.V., Andriyko L.S., Marynin A.I., Ukrainets A.I., Charmas B., Skubiszewska-Zięba J., Blitz J.P. Influence of hydrophobization of fumed oxides on interactions with polar and nonpolar adsorbates. *Appl. Surf. Sci.* 2017. **423**: 855.

37. Gun'ko V.M., Voronin E.F., Nosach L.V., Turov V.V., Wang Z., Vasilenko A.P., Leboda R., Skubiszewska-Zięba J., Janusz W., Mikhalovsky S.V. Structural, textural and adsorption characteristics of nanosilica mechanochemically activated in different media. *J. Colloid Interface Sci.* 2011. **355**(2): 300.

38. Turov V.V., Gun'ko V.M., Zarko V.I., Goncharuk O.V., Krupska T.V., Turov A.V., Leboda R., Skubiszewska-Zięba J. Interfacial behavior of n-decane bound to weakly hydrated silica gel and nanosilica over a broad temperature range. *Langmuir.* 2013. **29**(13): 4303.

39. Gun'ko V.M., Turov V.V., Zarko V.I., Pakhlov E.M., Charmas B., Skubiszewska-Zięba J. Influence of structural organization of silicas on interfacial phenomena. *Colloids Surf., A.* 2016. **492**: 230.

40. Mitchell J., Webber J.B.W., Strange J.H. Nuclear magnetic resonance cryoporometry. *Phys. Rep.* 2008. **461**(1): 1.

41. Petrov O.V., Furó I. NMR cryoporometry: Principles, applications and potential. *Progr. NMR Spectroscopy.* 2009. **54**(2): 97.

42. Aksnes D.W., Førland K., Kimtys L. Pore size distribution in mesoporous materials as studied by ^{1}H NMR. *Phys. Chem. Chem. Phys.* 2001. **3**(15): 3203.

43. Hay J.N., Laity P.R. Observations of water migration during thermoporometry studies of cellulose films. *Polymer.* 2000. **41**(16): 6171.

44. Landry M.R. Thermoporometry by differential scanning calorimetry: experimental considerations and applications. *Thermochim. Acta.* 2005. **433**(1–2): 27.

45. Weber J., Bergström L. Mesoporous hydrogels: revealing reversible porosity by cryoporometry, X-ray scattering, and gas adsorption. *Langmuir.* 2010. **26**(12): 10158.

46. Gun'ko V.M., Oranska O.I., Paientko V.V., Sulym I.Ya. Particulate morphology of nanostructured materials. *Him. Fiz. Tehnol. Poverhni.* 2020. **11**(3): 368.

47. Gun'ko, V.M. Textural characteristics of composite adsorbents analyzed with density functional theory and self-consistent regularization procedure. *Him. Fiz. Tehnol. Poverhni.* 2020. **11**(2): 163.

48. Gun'ko V.M., Turov V.V., Pakhlov E.M., Krupska T.V., Charmas B. Effect of water content on the characteristics of hydro-compacted nanosilica. *Appl. Surf. Sci.* 2018. **459**: 171.

49. Gun'ko V.M. Various methods to describe the morphological and textural characteristics of various materials. *Him. Fiz. Tehnol. Poverhni.* 2018. **9**(4): 317.

50. Gun'ko V.M. Nano/meso/macroporous materials characterization affected by experimental conditions and features of the used methods. *Him. Fiz. Tehnol. Poverhni.* 2020. **11**(1): 5.

51. Gun'ko V.M. Polymer adsorbents vs. functionalized oxides and carbons: particulate morphology and textural and surface characterization. *Polymers.* 2021. **13**(1249): 1.

52. *ImageJ.* Version 1.53m. 2021. https://imagej.nih.gov/ij/, https://imagej.nih.gov/ij/plugins/granulometry.html

53. *Fiji.* 2021. https://fiji.sc/, https://imagej.net/local_thickness

54. Gun'ko V.M. Morphological and textural features of various materials composed of porous or nonporous nanoparticles differently packed in secondary structures. *Appl. Surf. Sci.* 2021. **569**: 151117.

55. Gun'ko V.M., Matkovsky A.K., Charmas B., Skubiszewska-Zięba J., Pasieczna-Patkowska S. Carbon-silica gel adsorbents: effects of matrix structure and carbon content on adsorption of polar and nonpolar adsorbates. *J. Therm. Anal. Calorim.* 2017. **128**(3): 1683.